35th Annual International Conference of the IEEE EMBS
Osaka, Japan, 3 - 7 July, 2013

A Novel Coupling Algorithm for Computing Blood Flow in Viscoelastic Arterial Models

Lucian Itu[1,3], Puneet Sharma[2], Ali Kamen[2], Constantin Suciu[1,3], Dorin Comaniciu[2]

***Abstract*— We propose a novel coupling algorithm, based on the operator-splitting scheme, which implements the viscoelastic wall law at the coupling nodes of the vessels. Two different viscoelastic models are used (V1 and V2), leading to five different computational setups: elastic wall law, model V1 applied at interior and coupling grid points, model V1 applied only at the interior grid points (V1-int), model V2 applied at interior and coupling grid points, model V2 applied only at the interior grid points (V2-int). These have been tested with two arterial configurations: (i) single artery, and (ii) complete arterial tree. Models V1-int and V2-int lead to incorrect conclusions and to errors which can be of the same order as, and are at least 1/5 of, the difference between the results with the elastic and the viscoelastic laws. Both test cases demonstrate the importance of modeling the viscous component of the pressure-area relationship at all grid points, including the coupling points between vessels or at the inlet/outlet of the model.**

I. INTRODUCTION

Blood flow modeling of the cardiovascular system provides key insights about the conditions in blood vessels and is useful for diagnosis and surgical planning [1]. When the main focus lies on flow rate and pressure wave forms, one-dimensional models are efficient and have been shown to be able to accurately compute these quantities for patient-specific models [2], [3], [4]. Most of the 1-d models use elastic wall laws [5], [6], [7], while a few have also proposed viscoelastic wall models [8]. When an elastic wall model is used, a hyperbolic system of equations is obtained, which can be readily solved using second-order explicit methods. For viscoelastic wall models, the hyperbolic nature of the equations is lost and the approaches for the numerical solution of the equations can be divided into two main categories:

1) Approaches that do not exploit the hyperbolic nature of the equations (non-linear terms are solved iteratively using the Newton method) [2], [9], [10];
2) Approaches that recover the original hyperbolic nature by employing an operator-splitting scheme for the momentum equation [6], [8], [11].

The second approach is computationally efficient since it exploits the hyperbolic nature of the conservation equations, but it also introduces an approximation due to operator-splitting. Conflicting results were reported for the effect of the viscoelastic term: similar pressure waveform but a smaller area variation [9], and a higher pressure pulse but similar area variation [11]. The work in [8] and [11] neglected the viscous term in the wall law at the coupling nodes of the vessel segments (inlet, junction, outlet), which has been identified as a potential cause for the contradiction.

In this paper, we propose a novel coupling algorithm, based on the operator-splitting scheme, which implements the complete viscoelastic wall law at the coupling nodes of the vessels. We use two different formulations for the viscoelastic law and report the results for a single artery and a complete arterial model test case.

II. MATERIALS AND METHODS

A. Viscoelastic One-Dimensional Blood Flow Model

The quasi 1-d flow model consists of the mass and momentum conservation equations [5]:

$$\frac{\partial A}{\partial t} + \frac{\partial q}{x} = 0, \quad (1)$$

$$\frac{\partial q}{\partial t} + \frac{\partial}{\partial x}\left(\alpha \frac{q^2}{A}\right) + \frac{A}{\rho}\frac{\partial p}{\partial x} = K_R \frac{q}{A}, \quad (2)$$

where $A = A(x,t)$ is the cross-sectional area, p the pressure, and q the flow rate (spatial and temporal dependencies of the quantities have been omitted for notational clarity). Coefficients α and K_R account for the momentum-flux correction and viscous losses respectively. Additionally, a state equation relating the pressure in the vessel to the cross-sectional area is also specified. The vessel wall can be modeled as a Voigt-type material to include the viscoelastic effects [12]. The following two state equations have been proposed [8], [13]:

$$\text{Model V1: } p = \frac{4}{3}\frac{Eh}{r_0}\left(1 - \sqrt{\frac{A_0}{A}}\right) + \frac{\gamma_S}{A\sqrt{A}}\frac{\partial A}{\partial t} + p_0 \quad (3)$$

$$\text{Model V2: } p = \frac{4}{3}\frac{Eh}{r_0}\left(1 - \sqrt{\frac{A_0}{A}}\right) + \frac{\gamma_S}{A_0\sqrt{A}}\frac{\partial A}{\partial t} + p_0, \quad (4)$$

where E is the Young modulus, h is the wall thickness and r_0 is the initial radius corresponding to pressure p_0. The viscoelastic coefficient γ_S is set equal in both cases:

$$\gamma_S = \frac{T_S \cdot \tan\Phi_S}{4\pi}\frac{hE}{1-\sigma^2}, \quad (5)$$

where T_S is the wave characteristic time, Φ_S is the viscoelastic angle, and σ is the Poisson ratio. The numerical

[1]Transilvania University of Brasov, Brasov, Romania. Email: lucian.itu@unitbv.ro
[2]Imaging and Computer Vision, Siemens Corporation, Corporate Technology, Princeton, New Jersey, United States. Emails: {sharma.puneet, ali.kamen, dorin.comaniciu}@siemens.com
[3]Siemens Corporate Technology, Brasov, Romania. Email: constantin.suciu@siemens.com
*This work is partially supported by the program Partnerships in Priority Domains (PN II), financed by ANCS, CNDI - UEFISCDI, under the project nr. 130/2012.

solution method of the 1-d model is a domain decomposition approach, where the continuity of flow and total pressure is imposed at the coupling nodes. A time-varying flow rate profile is imposed at the inlet and 3-element Windkessel models are coupled at the outlets. For the numerical solution, we applied the Taylor series expansion using finite differences, which requires the equations to be written in conservation form. The presence of the viscoelastic term in (3)/(4) introduces an additional term in the momentum conservation equation. Using the mass conservation, (2) can be rewritten as:

$$\frac{\partial q}{\partial t} + \frac{\partial}{\partial x}\left(\alpha \frac{q^2}{A}\right) + \frac{A}{\rho}\frac{\partial \Psi_{el}}{\partial x} - \frac{A}{\rho}\frac{\partial}{\partial x}\left(\gamma \frac{\partial q}{\partial x}\right) = K_R \frac{q}{A} \quad (6)$$

Since (6) can no longer be cast into conservation form, the operator splitting scheme introduced in [6] has been applied. It assumes that the contribution of the viscoelastic term is small compared to that of the elastic term. The flow rate is considered to be composed of an elastic and a viscoelastic component ($q = q_e + q_v$), and (6) is split into two equations:

$$\frac{\partial q_e}{\partial t} + \frac{\partial}{\partial x}\left(\alpha \frac{q^2}{A}\right) + \frac{A}{\rho}\frac{\partial \Psi_{el}}{\partial x} = K_R \frac{q}{A} \quad (7)$$

$$\frac{\partial q_v}{\partial t} - \frac{A}{\rho}\frac{\partial}{\partial x}\left(\gamma \frac{\partial q}{\partial x}\right) = 0 \quad (8)$$

Consequently, the numerical solution at each step is composed of two sequential sub-steps:

- The system composed of (1) and (7) is solved, yielding the quantities $A(x,t)$ and $q_e(x,t)$;
- (8) is solved with homogeneous Dirichlet boundary conditions to obtain $q_v(x,t)$ and the total flow rate $q(x,t)$.

B. Coupling Algorithm

Previous works have neglected the viscoelastic component of the pressure at the coupling nodes [8], [11]. To determine the validity of this assumption, we have developed a novel iterative implicit coupling algorithm, that is applied to inflow, bifurcation and outflow points. The algorithm is a generalization of the one introduced in [14] and can be applied for the coupling of m domains (one upstream domain, referred by subscript index 1, and $m-1$ downstream domains). The models of these domains may be of any geometrical scale (3D/1D/0D). For the upstream model, a pressure boundary condition is used, while for the downstream models a flow rate boundary condition is applied. Superscript n refers to the solution at time step t^n, and k refers to the iterations performed at each time step to enforce the continuity of flow and total pressure.

1) Initialization: $k=0$, $q_{i,0}^{n+1} = q_i^n, p_{i,0}^{n+1} = p_i^n, A_{i,0}^{n+1} = A_i^n, i = 1 \dots m$.
2) Loop on k
   a) Compute the total flow rate to be distributed between the downstream vessels: $q_{2\div m,k+1}^{n+1} = \chi q_{1,k}^{n+1} + (1-\chi)\sum_{i=2}^{m} q_{i,k}^{n+1}$ where χ is a relaxation parameter.
   b) Solve the downstream models using the following set of conditions: $\sum_{i=2}^{m} q_{i,k+1}^{n+1} = q_{2\div m,k+1}^{n+1}$ $p_{i,k+1}^{n+1} = p_{i+1,k+1}^{n+1}, i = 2 \dots, m-1$. As a result $p_{i,k+1}^{n+1}$ and $q_{i,k+1}^{n+1}$ for $i = 2 \dots m$, are computed.
   c) Solve the upstream model using the boundary condition $p_{1,k+1}^{n+1} = p_{2,k+1}^{n+1} \rightarrow q_{i,k+1}^{n+1}$. Set $k = k+1$.
3) Convergence: if, $\left| q_{1,k+1}^{n+1} - \sum_{i=2}^{m} q_{i,k+1}^{n+1} \right| < \epsilon$, then advance to step 1, else go to step 2.

Next, we introduce a set of additional remarks regarding the application of this algorithm for the coupling between 1-d domains (the algorithm is applied during step 1 of the operator-splitting scheme). Given a certain pressure for the pressure boundary condition at step 2.c, the area at the outlet point of the upstream vessel, $A_{1,k+1}^{n+1}$, needs to be determined. To compute the inverse of (3)/(4), the discretized equations are used:

$$p_{1,k+1}^{n+1} = \frac{4}{3}\frac{Eh}{r_0}\left(1 - \sqrt{\frac{A_0}{A_{1,k+1}^{n+1}}}\right) + \gamma \frac{A_{1,k+1}^{n+1} - A_1^n}{\Delta t} + p_0 \quad (9)$$

$$\gamma = \frac{\gamma_S}{A_0 \sqrt{A}_{1,k+1}^{n+1}} \quad or \quad \gamma = \frac{\gamma_S}{A_{1,k+1}^{n+1} \sqrt{A}_{1,k+1}^{n+1}} \quad (10)$$

Equation (9) is solved using the Newton method and the unknown $A_{1,k+1}^{n+1}$ is initialized with the value from the previous iteration $A_{1,k}^{n+1}$.

If the algorithm is used to couple two vessels, or to couple a vessel and a Windkessel model, i.e. $m = 2$, step 2.b is simplified since the flow rate to be imposed for the downstream vessel is determined directly. If $m > 2$, a system of $m-2$ nonlinear equations is obtained, that is solved using the Newton method. The negative characteristic can be cast into the following form for each downstream vessel: $q_{i,k+1}^{n+1} = c_{i1} \cdot A_{i,k+1}^{n+1} - c_{i2}, i = 2, \dots, m.$ where c_{i1} and c_{i2} are constants. Thus,

$$A_{m,k+1}^{n+1} = \frac{1}{c_{m1}}\left(q_{2\div m,k+1}^{n+1} - \sum_{i=2}^{m-1}(c_{i1} \cdot A_{i,k+1}^{n+1} - c_{i2}) - c_{m2}\right).$$

Finally, the inlet flow rate of each downstream vessel is computed. For a regular bifurcation, i.e. m = 3, a single nonlinear equation is obtained. Although the coupling algorithm refers to one upstream vessel and $m-1$ downstream vessels, there is no restriction regarding the direction of the flow.

III. RESULTS

Blood was modeled as an incompressible Newtonian fluid with density $1.055\, g/cm^3$ and a dynamic viscosity $0.045\, dynes/cm^2 s$. The parameters of γ_S were set as follows: $T_S = 0.30\, s$, $\Phi_S = 10$, $\sigma = 0.5$. Coupling nodes were solved using the algorithm introduced in Section II. Parameter χ was set to 0.5 and the tolerance threshold for the coupling algorithm and the Newton iterations was set to 10^{-8}. A gridspacing of $0.1\, cm$ and a time-step of $5 \times 10^{-5}\, s$ was used. Simulations were run for 15 cycles to guarantee convergence. Five computational setups were used: (a) elastic

wall law, (b) model V1 applied at interior and coupling grid points, (c) model V1 applied only at the interior grid points (V1-int), (d) model V2 applied at interior and coupling grid points, and (e) model V2 applied only at the interior grid points (V2-int). These were tested with two arterial configurations: (i) single artery, (ii) complete arterial tree. We also compared the results obtained with the classic coupling algorithm based on the method of characteristics [5] with the results obtained with the coupling algorithm in section 2.b (using an elastic wall law). We computed the L_2 norm of the absolute differences between the two solutions. The norm results were in the order of $10^{-6}cm^2$ for the area, $10^{-5}ml/s$ for the flow rate, and $10^{-5}mmHg$ for the pressure, showing that both coupling algorithms lead to the same results.

A. Single Artery Case

This test case consisted of an arterial segment with a length of $3.0cm$ and a radius of $1.25\,cm$. An analytical time-varying flow rate profile, given by an asymmetric Gaussian function with an average value of $80\,ml/s$, was imposed at the inlet. The Windkessel parameters of the outlet boundary condition were: $R_p = 100\,dynes\,s/cm^5, R_d = 1500\,dynes\,s/cm^5, C = 1.3 \cdot 10^{-3}\,cm^5/dynes$. The results are displayed in Figure 1 for the mid-vessel cross-section (at $1.5\,cm$) and are summarized in Table I. When the viscous component in the pressure-area relationship is modeled at all grid points, the pressure is almost unaffected, and a lower cross-sectional area variation is obtained. Conversely, when the viscous component is modeled only at the interior points, the pressure pulse is higher and the cross-sectional area variation is similar to the elastic case. The time-to-peak of the pressure is unchanged for models V1 and V2 but decreases for models V1-int and V2-int. The peak-value of the cross-sectional area is reached at a later moment in time.

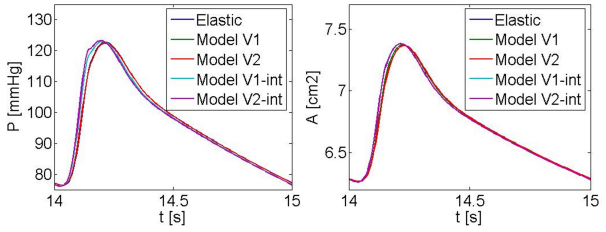

Fig. 1. Comparison of time-varying pressure and cross-sectional area for the single artery test case, obtained when applying the elastic model, and models V1, V2, V1-int and V2-int.

TABLE I

DIFFERENCES IN PRESSURES AND CROSS-SECTIONAL AREAS FOR THE SINGLE ARTERY TEST CASE.

Measuremenet	Elastic	V1	V2	V1-int	V2-int
$P_{max} - P_{min}$ $[mmHg]$	46.39	46.35	46.36	47.18	47.51
$A_{max} - A_{min}$ $[cm^2]$	1.118	1.086	1.079	1.117	1.118
t_{peak} $[s]$	0.215	0.215	0.215	0.203	0.196

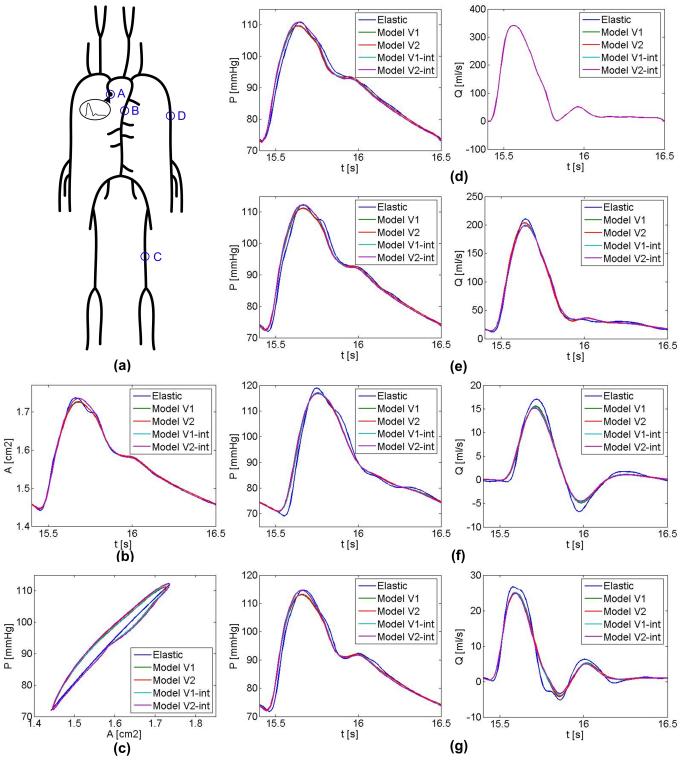

Fig. 2. (a) Human arterial tree model composed of 51 arteries, (b) Time-varying cross-sectional area at the descending aorta, (c) Pressure-area variation at the descending aorta, (c-f) Time-varying pressure and flow rate at the aortic root, descending aorta, femoral artery and subclavian artery.

B. Full Body Arterial Tree Case

A complete arterial tree with 51 segments based on [15], was used for this case. Figure 2a shows the vascular tree, together with the 4 locations (marked with letters A-D), at which the time-varying pressure and flow rate values are displayed in Figure 2d-g. The viscoelastic effects dampen the high-frequency oscillations in the pressure and flow waveforms, a phenomenon which is more pronounced at the distal locations. These observations are consistent with results reported in literature [2]. Furthermore pressure and area were out of phase, the peak cross-sectional area value being generally reached at a later moment in time (Figure 2b). A smaller cross-sectional area variation was obtained for models V1 and V2, whereas for models V1-int and V2-int, the variation is similar to the one obtained with the elastic law. For completeness, Figure 2c displays the hysteresis obtained in the pressure-area relationship at the same location. Results are similar for models V1 and V2. To quantify the difference between the results obtained with models V1 and V1-int, and with models V2 and V2-int, we computed the average and maximum relative differences at locations A-D (Figure 2a). We also computed the average and maximum relative differences between the results obtained with models V1 and V2, and with the elastic model. The errors are displayed in Table II. Although the differences between models V1 and V1-int and V2 and V2-int respectively are small, they are comparable to the differences between the

TABLE II

RELATIVE AVERAGE AND MAXIMUM DIFFERENCES OBTAINED BETWEEN DIFFERENT IMPLEMENTATIONS OF THE VISCOELASTIC MODELS, AND BETWEEN THE VISCOELASTIC AND ELASTIC MODELS, AT LOCATIONS A-D DISPLAYED IN FIG. 2A.

Artery	Diff	V1 – V1-int		V1 – elastic		V2 – V2-int		V2– elastic	
		P[%]	Q[%]	P[%]	Q[%]	P[%]	Q[%]	P[%]	Q[%]
Asc.	Avg.	0.545	0.0	0.954	0.0	0.620	0.0	1.088	0.0
Aorta	Max.	1.227	0.0	3.896	0.0	1.397	0.0	4.353	0.0
Desc	Avg.	0.499	0.851	0.897	1.343	0.568	0.956	1.019	1.472
Aorta	Max.	0.961	2.970	3.955	3.447	1.100	3.289	4.410	3.887
Femoral	Avg.	0.310	0.984	1.528	3.866	0.342	1.079	1.697	4.278
Artery	Max.	1.104	3.030	7.812	11.66	1.241	3.365	8.484	12.96
Subcl.	Avg.	0.522	1.019	1.128	3.982	0.594	1.090	1.287	4.387
Artery	Max.	1.231	3.417	5.774	17.74	1.390	3.652	6.365	19.12

viscoelastic and elastic model. Even for the distal locations, where the influence of the viscous component is higher, neglecting the viscous component in the wall law at the coupling points introduces errors which represent 1/5 or more of the difference between the viscoelastic and the elastic models.

IV. CONCLUSIONS

We have introduced a novel coupling algorithm which can be equally applied to implicitly couple inflow, bifurcation and outflow points in 1-d and multiscale models. The primary goal of this coupling algorithm was to consider the viscous component in the wall law at the coupling points and not only at the interior points of an arterial segment. For simple geometries, the consideration of the viscoelastic law at the coupling points leads to lower variations in pressure and cross-sectional area. Moreover, pressure and flow rate are comparable to the results obtained with the elastic law, and only the cross-sectional area has a different time-dependent behavior. Similar conclusions have been obtained recently in [9] for relatively simple geometries (carotid artery and abdominal aorta model).

For the full arterial tree model, viscoelasticity leads to changes of up to 6% in the pressure values and up to 20% in the flow rate values. The errors introduced by models V1-int and V2-int can be of the same order as, and are at least 1/5 of, the difference between the results with the elastic and the viscoelastic laws. Results have been consistent for both viscoelastic models.

Both test cases demonstrate that it is important to consider and to implement the viscous component of the pressure-area relationship at all grid points, including the coupling points between vessels or at the inlet/outlets of the model. Models V1-int and V2-int have led to incorrect conclusions and to significant numerical errors, which are independent of the viscoelastic law ((3) or (4)). Hence, although the operator splitting introduces an approximation, it leads to the correct results and conclusions, but only if the viscoelastic law is implemented properly at all grid points and not only at the interior points.

REFERENCES

[1] C. Taylor and D. Steinman, "Image-based modeling of blood flow and vessel wall dynamics: Applications, methods and future directions," *Annals of Biomedical Engineering*, vol. 38, pp. 1188–1203, 2010.

[2] P. Reymond, Y. Bohraus, F. Perren, F. Lazeyras, and N. Stergiopulos, "Validation of a patient-specific one-dimensional model of the systemic arterial tree," *American Journal of Physiology - Heart and Circulatory Physiology*, vol. 301, no. 3, pp. H1173–H1182, 2011.

[3] L. Itu, P. Sharma, V. Mihalef, A. Kamen, C. Suciu, and D. Comaniciu, "A patient-specific reduced-order model for coronary circulation," in *Biomedical Imaging (ISBI), 2012 9th IEEE International Symposium on*, may 2012, pp. 832 –835.

[4] L. Itu, P. Sharma, K. Ralovich, V. Mihalef, R. Ionasec, A. Everett, R. Ringel, A. Kamen, and D. Comaniciu, "Non-invasive hemodynamic assessment of aortic coarctation: Validation with in vivo measurements," *Annals of Biomedical Engineering*, pp. 1–13, 2012.

[5] M. S. Olufsen, C. S. Peskin, W. Y. Kim, E. M. Pedersen, A. Nadim, and J. Larsen, "Numerical simulation and experimental validation of blood flow in arteries with structured-tree outflow conditions," *Annals of Biomedical Engineering*, vol. 28, pp. 1281–1299, 2000.

[6] L. Formaggia, D. Lamponi, and A. Quarteroni, "One-dimensional models for blood flow in arteries," *Journal of Engineering Mathematics*, vol. 47, pp. 251–276, 2003.

[7] J. P. Mynard and P. Nithiarasu, "A 1d arterial blood flow model incorporating ventricular pressure, aortic valve and regional coronary flow using the locally conservative galerkin (lcg) method," *Communications in Numerical Methods in Engineering*, vol. 24, no. 5, pp. 367–417, 2008.

[8] J. Alastruey, A. W. Khir, K. S. Matthys, P. Segers, S. J. Sherwin, P. R. Verdonck, K. H. Parker, and J. Peir, "Pulse wave propagation in a model human arterial network: Assessment of 1-d visco-elastic simulations against in vitro measurements," *Journal of Biomechanics*, vol. 44, no. 12, pp. 2250 – 2258, 2011.

[9] R. Raghu, I. E. Vignon-Clementel, C. A. Figueroa, and C. A. Taylor, "Comparative study of viscoelastic arterial wall models in nonlinear one-dimensional finite element simulations of blood flow," *Journal of Biomechanical Engineering*, vol. 133, no. 8, p. 081003, 2011.

[10] D. Bessems, C. G. Giannopapa, M. C. Rutten, and F. N. van de Vosse, "Experimental validation of a time-domain-based wave propagation model of blood flow in viscoelastic vessels," *Journal of Biomechanics*, vol. 41, no. 2, pp. 284 – 291, 2008.

[11] T. Passerini, "Computational hemodynamics of the cerebral circulation: multiscale modeling from the circle of Willis to cerebral aneurysms," Ph.D. dissertation, Politecnico di Milano, Italy, 2008.

[12] Y. C. Fung, *Biomechanics: mechanical properties of living tissues*. Berlin: Springer, 1993.

[13] A. C. I. Malossi, P. J. Blanco, and S. Deparis, "A two-level time step technique for the partitioned solution of one-dimensional arterial networks," *Computer Methods in Applied Mechanics and Engineering*, vol. 237240, no. 0, pp. 212 – 226, 2012.

[14] T. Passerini, M. Luca, L. Formaggia, A. Quarteroni, and A. Veneziani, "A 3d/1d geometrical multiscale model of cerebral vasculature," *Journal of Engineering Mathematics*, vol. 64, pp. 319–330, 2009.

[15] N. Stergiopulos, D. Young, and T. Rogge, "Computer simulation of arterial flow with applications to arterial and aortic stenoses," *Journal of Biomechanics*, vol. 25, no. 12, pp. 1477 – 1488, 1992.